RSC Advances

ROYAL SOCIETY OF CHEMISTRY

www.rsc.org/advances

Themoxidative stability and char formation mechanism for the introduction of

CNTs and MoS$_2$ into halogen-free flame retarding TPEE

Wei Wu *, Maolin Li, Yuhua Zhong*,Mengjingzi Zong, Shengdong Xiao, Xiuhan Li,

Fuyan Xie,

Sino-German Joint Research Centre of Advanced Materials, School of Materials and

Engineering, East China University of Science and Technology, Shanghai, 200237,

PR China

*Corresponding author: Wei Wu. Tel./fax: 021-64253480. E-mail:

wuwei@ecust.edu.cn.

Yuhua Zhong. Tel/fax:021-64250850. E-mail:

zhongyuhua890101@hotmail.com

Abstract

In this paper, we give an insight to the char formation mechanism for the

addition of CNTs and MoS$_2$ into halogen-free flame retarding thermoplastic

poly(ether ester) elastomer (TPEE). We used the real-time Fourier transform infrared

spectroscopy (FTIR) to analyze the change of the characteristic peaks of formulations

during the themoxidative process. Thermoxidative stability of the samples was

investigated by thermalgravimertic analysis (TGA) under air atmosphere at a heating

rate of 10 ^{o}C min^{-1}. The catalyzation of carbon nanotubes (CNTs) during the

themoxidative process was demonstrated. The pyrolysis products for different

formulations were studied by Pyrolysis/gas chromatography/mass spectroscopy

(Pyrolysis/GC/MS). The variation of composition of the volatile decomposition

product (Mn< 100 g/mol) was discussed. The morphology and the graphite degree of the high temperature remained residues was studied by scanning electronic morphology (SEM) and Raman Spectra, respectively. We found that the Mo element can catalyze effectively the char forming process through the cycloaddition interaction of volatile decomposition products. TPEE/P-N/CNTs/MoS$_2$ has the best stable char structure for the combination of the bone structure of CNTs and the cycleaddition reaction of the pyrolysis gas products with the low molecular weight.

Keywords: Carbon nanotubes; Molybdenum disulfide; flame retardant;

1. Introduction

Thermoplastic poly(ether ester) elastomer (TPEE) is a potential polymer material which can replace the natural and synthetic rubber.[1] With the combination of advantages of flexibility of rubber, the strength of plastics, and the processibility of thermoplastics, TPEE has been widely used for various applications.[2] The development of multifunctional TPEE with excellent performance has been a hotspot research topic. Much efforts has been done to realize this goal such as the incorporation the functional groups in the main chain of TPEE,[3-6] the preparation of the TPEE alloy and TPEE nanocomposites.[7-9] Meanwhile TPEE is easily ignited and burned with serious melt dripping behavior and the release of combustible decomposition products[10] which limit its application in many fields. To enhance the flame retarding performance to meet the requirement of industrial application is urgent. The formation of a compacted char during the burning process has proven to

be an effective way to enhance the fire retardancy of polymer.[11-13] In recent years, the incorporation of nanofillers with a high aspect ratio can enhance the flame retardancy of the polymer obviously on account for the formation of a high-quality char during the burning process.[14, 15]

Carbon nanotubes (CNTs) have been attracted considerable interest due to their unique structure, electronic, thermal and mechanical properties[16] and, thus have been used in various applications, including drug delivery[17, 18], chemical sensor[19, 20], electronic sensor[21, 22] and reinforced fillers for polymer[23, 24]. CNTs have been a promising candidate for enhancing the flame retardancy of polymer materials since 2002.[25] The published literatures showed that the introduction of CNTs into the polymer can effectively improve the thermal stability and flame retardant of composite for it can provide the barrier effect for the matrix during the heating process[26-29]. Further, the combination of CNTs and other nanoadditives exhibited a synergistic effect in the formation of the char at the high temperature.[30-33]

Meanwhile, in recent years, molybdenum disulfide (MoS_2), a type of two-dimensional (2D) layered materials, has attracted more and more attentions from various applications such as transistors[34], catalysts[35], composites[36, 37] due to its intrinsic structure and unique performances. MoS_2 was called white graphite for the similar structure like graphite. Different layers were associated by van der Waals forces.[38-40] Recently, MoS_2 was incorporated into polymer materials to enhance the fire resistance and thermal stability.[41-44]

The dominated synergistic flame retarding mechanism of CNTs and MoS_2 is that

the formation of the three-dimensional (3D) network structure in matrix which can provide the physical nano-barrier effect and act as framework structure during the burning process resulted in the enhancement of the thermal stability and flame resistance of the nanocomposites. Nanofillers play the physical role during the char formation process.

However, the chemical interaction of the CNTs and MoS_2 the char formaiton process has not yet been reported so far. The aim of this study was to give an insight to the thermoxidative decomposition and the char forming mechanism for the introduction of the combination of CNTs and MoS_2 into halogen-free flame retarding TPEE. MoS_2 can eliminate the negative effect of CNTs on the chemical char forming process. The new flame retarding mechanism would provide guidance to develop the next generation of a binary synergist system.

2. Experimental

2.1 Materials

TPEE (H3303) was provided by Sunplas (China). P-N flame retardant consists of diethylphosphinate (AlPi) and melamine polyphosphate (MPP) were provided by Clariant (German), the mass ratio of AlPi and MPP is 2:1. Carbon nanotubes (CNTs, with purity >95%, length: 0.5-40 μm, diameter: 10-30 nm, Ni ~ 2.4%, Fe ~ 0.4%) and Molybdenum disulfide (MoS_2, AP, particle size ~3 μm, the density: 5.06 g/ml) were purchased from Shenzhen Nanotech Port Co.,LTD and Sigma-Aldich, respectively. CNTs and MoS_2 were used as received without any chemical treatments. Table 1 showed the composition of the different formulations. All the formulations melted in a

twin-roll mill at 190 ^{o}C for 10 minutes with the screw speed of 60 rpm. All the

materials were hot-pressed under 12 MPa for 5 min at about 190 ^{o}C for the sheet of

the suitable thickness and size for analysis.

(Here Table 1)

2.2 Measurements

2.2.1 Dripping behavior

Samples were measured by UL 94 (ASTM D3801, Size of the sample: 130

mm×13 mm×1.6 mm.)

2.2.2 Residues Analysis

High temperature remained residues are collected from the samples after heating

treatment at 800 ^{o}C for 10 min., . The morphology of the residues were observed by

using SEM (S-4800, Hitachi, Japan). The degree of the graphitization was calculated

by the results of Laser Raman spectroscopy (LRS) measurements. Raman spectra

were recorded at room temperature on an SPEX-1403 laser Raman spectrometer with

a 200 mW argon-ion laser at an excitation wavelength of 514.5 nm.

2.2.3 Thermoxidative stability

Thermogravimetry analysis (TGA) was measured by using a NETZSCH STA 409

PC/PG thermogravimetry analyzer in air atmosphere with a heating rate of 10 ^{o}C

min^{-1}.

2.2.4 FTIR spectroscopy

The change of the characteristic peaks during the heating process was measured

by Fourier transform infrared (FTIR) spectra with a heating device. Samples filmed

on a KBr disc were heated from room temperature to 400 $^{\circ}$C with a heating rate of

10°C min^{-1}.

2.2.5 Pyrolysis/GC/MS analysis

To investigate the volatile product during the burning test, formualtion 1-4 were

analyzed by pyrolysis/gas chromatogram/mass spectrometry (pyrolysis/GC/MS). The

samples were pyrolyzed at 600 $^{\circ}$C. The gas thermal decomposition products were

identified by GC/MS (Agilent 6890/5073B). Mass range: 18~500 amu.

3. Result and discussion

3.1 Dripping behavior

(Here Table 2)

The results of UL 94 tests of all the formulations were shown in Table 2. As

presented in our previous research, TPEE burned with heavily melt dripping

phenomenon in the UL 94 test. Meanwhile, the P-N flame retardant can't form the

compacted char with enough strength to protect the matrix to prevent the heat and

mass transfer.[10] Melt dripping behavior was still existed by simply adding the P-N

flame retardant into TPEE. With the addition of 3wt% CNTs into P-N flame retarding

TPEE can't get the desirable fire resistance without melt dripping behavior. However,

adding the combination of CNTs and MoS_2 into TPEE with P-N flame retardants got

the V-0 ranking. The significant difference in UL 94 test between TPEE/P-N/CNTs

and TPEE/P-N/CNTs/MoS_2 was highlighted in the result of the dripping behavior.

TPEE/P-N/CNTs presented the melt dripping behavior during the first ignition

process of UL 94 tests. TPEE/P-N/CNTs/MoS_2 leads to the best flame retardancy in

terms of anti-dripping behavior. The reason for the different results of UL 94 test for

TPEE/P-N/CNTs and TPEE/P-N/CNTs/MoS$_2$ will be discussed in the following part.

3.2 Thermoxidative decomposition and chain formation mechanism

3.2.1 Real time FTIR

Fig.1 showed the alternation of the intensity and wavenumber of characteristic

peaks of the solid phase in FTIR spectra at a heating rate of 10 ^{o}C min^{-1} in the air

atmosphere. All the attributions of wavenumbers for the typical bands were presented

in Table. 3. The changes of characteristic bands of TPEE during the decomposition

process were given in Fig.1 (a). The intensities of band at 2956 and 2861 cm^{-1} (-CH$_2$)

decreased rapidly at the high temperature mainly resulted from the chain scission of

the α-methylene group in the soft segment which was demonstrated in our previous

work[10]. In Fig.1 (b), the characteristic band at 3413 cm^{-1} is attributed to the action of

the intermolecular hydrogen bond of MPP. As increased with the temperature, there

are no peaks at 3300~3600 cm^{-1} resulted in the release of the non-flammable gas like

ammonium. During the heating process, the metal ions interacted with the

decomposition products containing carbonyl acid groups. The typical absorption

bands of carboxyl (C=O) (1715 cm^{-1}) shifted to the lower wavenumbers (1683 cm^{-1})

for the migration of electrons for the interaction with the metal ions for the

introduction of flame retardant. P-N flame retardants changed into metal

polyphosphate salt formed a brittle char with the different size holes on the surface of

the matrix.[10]

However, the characteristic band of CNTs and MoS$_2$ is hard to be observed for

their low amount addition and the method of sample preparation for the FTIR test. The changes of typical peaks for Formulation 3 were shown in Fig.1 (c). With addition of 3wt% CNTs into TPEE/P-N composites, TPEE/P-N/CNTs failed in the UL 94 tests for the melt dripping behavior. The anti-dripping performance of TPEE/P-N/CNTs was even worse than that of TPEE/P-N for the appearance of melt dripping behavior at the first ignition process of UL 94 tests. As we all know, CNTs can effectively increase the viscosity with regarding to the formation network structure.[45]

The only typical band at 1675 cm^{-1} was attributed for the electric charge on the metal ion to the carboxyl group. There might be two points to the change of the peak. The first one is the metal cation on the surface of the CNTs and the Aluminum ion (Al^{3+}) acts as Lewis acid sites, providing the basis for a coordinative interaction with the carbonyl group of TPEE. The introduction of CNTs can strengthen the Lewis based-acid interaction between the additives and the decomposition products. The other point is that the barrier effect can decrease the release rate of the degradation products. Therefore, the Aluminum ion (Al^{3+}) can react with the decomposition products containing the carbonyl group completely for the barrier effect provided by the network structure of CNTs. There is another interesting zone at 2800~3000 cm^{-1} in the meantime. The characteristic peaks of aliphatic groups completely disappeared at the high temperature, indicating the addition of CNTs accelerated the chain scission reaction resulted from the existence of the metal ion on the surface of CNTs which was corresponded to the composition of CNTs. However, the burning process is a

vigorous chemical and physical reaction with the release of heat and volatile gases. The barrier effect provided by the introduction of CNTs can enhance the thermal stability. Meanwhile, the catalyzation of the metal ions on the surface of CNTs can accelerate the chain scission reaction. As the result of UL 94 tests, we found that the catalyzation of CNTs is the main course of the melt dripping behavior. The introduction of CNTs also can't result in the formation of the compacted stable char to prevent the melt dripping behavior. Then, we moved on Formulation 4. The alternation of characteristic bands of TPEE/P-N/CNTs/MoS$_2$ during the heating process is presented in Fig.1 (d). There are two obvious distinctive regions in the spectra comparing with TPEE/P-N/CNTs. The intensity of typical bands at 2800~3000 cm^{-1} of the aliphatic groups at 400 ^{o}C indicating the introduction of MoS$_2$ revealed the decomposition rate of aliphatic groups of TPEE resulted from the decomposition catalyzation for the addition of CNTs. The second different region was in 1600~1750 cm^{-1}.

As presented in the Fig.1 (c), the characteristic peak of carboxyl group shifted to 1675 cm^{-1} completely for the interaction between the metal ions and the carboxyl acid. The special structure of TPEE/P-N/CNTs/MoS$_2$ decreases the decomposition rate during the heating process. For the better nano-barrier effect providing by 1-Dimensional CNTs and 2-Dimensional MoS$_2$ layers, which can promote the interaction between the additive and the decomposition products of TPEE, the characteristic peak of the carbonyl group should shift to the lower wavenumbers. The introduction of MoS$_2$ can promote the char formation and improving the char residue

was reported by other searchers.[41, 42]

The mechanism has not been demonstrated. If the Mo element might promote the char formation through the Lewis based-acid interaction (Fig.2(a), the characteristic peak of the carbonyl group should shift to the 1675 cm^{-1} completely. On the contrary, there are still two typical peaks in the 1630~1750 cm^{-1} zone indicating that the char formation process might be changed after the introduction of MoS_2. The double-bonded products undergo cycloaddition interaction for the catalyzation of Mo element improving additional carbonaceous char at the high temperature. The mechanism was given in Fig.2 (b). Thus, TPEE/P-N/CNTs/ MoS_2 has best stability corresponded the result of TG. These results attributed to the introduction MoS_2: the better nano-barrier effect for the coexistence of the CNTs and MoS_2 and the MoS_2 can promote char formation to avoid the catalysis of decomposition for the impurity on the surface of CNTs. The network structure reduces the release rate of the volatile gases which can provide more time for the char formation process.

3.2.2 Pyrolysis/GC/MS analysis

The thermal decomposition of Fomulation 1-4 in solid phase was investigated by real-time FIIR. Different kinds of product having carboxylic acid, hydroxyl end groups such as benzoic acid, tetrahydrofuran and their derivative mainly resulted from the degradation step of neat TPEE is the ester-linkage breaking reaction are released at the high temperature.[10]

(Here Fig.1)

This paper mainly focused on the change of the volatile product for the introduction

of P-N flame retardant, CNTs and MoS_2. In Fig.3, the introduction of the additives

didn't change the decomposition pathway of TPEE by comparing the peaks in the GC

spectra. All the various volatile products for the characteristic peaks was analyzed by

using Wiley's library. The identifications of the volatile products were presented in

Table 4. There are two characteristic peaks (7,9) were found for the introduction of

nitrogen containing flame retardant which resulted from the gas flame retarding action

of P-N flame retardant. The phosphorus containing products wasn't found

demonstrating that phosphorus containing flame retardant play flame retarding action

in solid phase. The characteristic mass peaks (Mn<100) and relative peak area of

Formulation 1-4 was presented in Table.5. The relative peak areas of low molecular

weight products were decreased after the introduction of additives. The value of

relative peak area of benzoic acid of TPEE/P-N/CNTs is 4.9 resulted from the

Lewis-based interaction between the benzoic acid and Ni^{2+} on the surface of the CNTs

corresponding the result of FITR. The value of relative peak area of 1,3-butadiene of

TPEE/P-N/CNTs/MoS_2 was half that of neat TPEE which indicated more

1,3-butadiene remained in the solid phase. The combination of the CNTs and MoS_2

effectively decreased the released of the 2,3-dihydrofuran and tetrahydrofuran

resulted from the chain scission of the α-methylene group in the soft segment due to

the nano-barrier effect of the 3-dimensional network.

(Here Fig.2)

The introduction of MoS_2 can decrease the release of the volatile product into gas

phase for the special nanostructure and the double-bonded containing product

remained in condensed phase for the catalyzation of char forming process. Therefore, TPEE/P-N/CNTs/MoS$_2$ has the best thermal stability and fire resistance.

(Here Fig.3)

(Here Table 3-5)

3.3 Thermoxidative performance

The thermoxidative behaviors of all the formulations were investigated by TG in the air atmosphere at a heating rate of 10 ^{o}C min^{-1}; the results are presented in Fig.4. As is showed in the picture, all the samples decomposed into two step thermal decomposition process, which means the additives didn't change the main decomposition pathway of TPEE. The thermoxidative behaviors of TPEE and TPEE/P-N were demonstrated in our previous research[10].

TPEE has no remained residues at 700 ^{o}C for the completely decomposition process. A special shoulder peak was observed at 300-350 ^{o}C which resulted from the chain scission of the α-methylene group of soft segments corresponding to the result of the real-time FTIR testing. The temperature of the shoulder peak, the first maximum decomposition temperature and the second maximum temperature all shifted to higher temperature than that of TPEE. The remained residue of TPEE/P-N increased to 8.5 wt%. The decomposition products of P-N flame retardant interact with the decomposition product of TPEE which effectively decreased the release of volatile products and enhance the thermal stability and remained residues at the high temperature.

Adding 3 wt% CNTs into P-N flame retarding TPEE, the initial decomposition temperature and the maximum decomposition temperature are higher than that of

TPEE/P-N which resulted from the barrier effect of CNTs.   However, the residue of

Formulation 3 at the end of the TG test decreases plainly to 6.81 wt%. Meanwhile, the

mass loss rate obviously increased since the introduction of CNTs. The results

suggested that the metal cation on the surface of CNTs catalyze the decomposition

process of TPEE during the thermoxidative heating process. While, adding 1 wt%

MoS_2 into TPEE/P-N/CNTs, the initial decomposition and the maximum

decomposition temperature was shifted to higher temperature. The remained residue

of Formulation 4 increased to also twice that of Formulation 3. The most interesting

thing is that the mass loss rate decreased obviously by simply adding 1 wt% MoS_2.

The result suggested that the combination of CNTs and MoS_2 can enhance the

network structure to improve the thermal stability of the nanocomposites for the

excellent barrier effect[45].

Besides, the increase of remained residue at the high temperature was attributed to the

interaction of the pyrolysis products and MoS_2 during the heating process.

3.4 Characterization of Residues

We got the residue after burning the samples in a muffle furnace at 800 $^{\circ}$C for 10

min. We found that there is no residue remained at a high temperature for neat TPEE.

The result corresponds with the results of TG. Fig.5 presents SEM images of the

residues of Formulation 2-4. The residue morphology of TPEE/P-N is given in Fig.5

(a). There are a lot of holes with different size presented in the image. The inner part

of the char has many porous structures which could be destroyed easily. During the

burning process, the release of the volatile products would be through the pathway of

the permeable holes and flaws. These brittle char can't protect the materials from the melt dripping behavior.

The residue morphology of TPEE/P-N/CNTs was presented in Fig.5 (b). We found that there is still different sized pores existed in the image. The char layer seems to be more compacted and integrated than that of TPEE/P-N. The introduction of CNTs into the composites resulted in the formation of network. The network structure can slow down the release rate of the composites for the barrier effect at the low temperature. At the high temperature, the CNTs can act as framework structure for building compacted char. Nevertheless, there are still many small holes in the char and the catalyzation of metal ions on the surface of CNTs resulted in the melt dripping behavior so as to reach V-2 ranking in the UL94 test.

The SEM images of the remained residue of TPEE/P-N/CNTs/MoS_2 are given in Fig.5(c). The introduction of MoS_2 has a clear improvement on the quality of the residue. The compacted structure can effectively stop the melt dripping behavior for it is strong enough to protect the matrix from the burning process. The results indicated that CNTs and MoS_2 had a good synergistic char formation effect since the formation of better network structure provide the excellent nano-barrier effect during the burning process.[41] The structure can decrease the release of volatile combustible products. And The CNTs can provide the framework structure and Mo element can catalyze the char forming process resulted in the compacted and dense char layer on the surface of the matrix.

As it is known to all, Laser Raman spectroscopy has been demonstrated as an

easy way to characterize the degree of graphitization of carbonaceous structure after burning process. As presented in the Fig.6, there are two bands existed for Formulation 2-4. The first one at 1352 cm^{-1} called D resulting from the amorphous carbon band, and the second one at 1600 cm^{-1} called G band resulting from the graphite crystalline. The degree of graphitization of the residual char could be calculated by the ratio of accumulated intensity of the D and G bands (I_D/I_G)[42].

Where I_D and I_G are the integrated intensities of the D and G bands, respectively. The residue has the lower ratio of I_D/I_G indicating the higher degree of graphitization and the better compacted char. Residue char layer with high degree of graphtization can efficiently decrease the rate of releasing volatiles products for the integrated structure during the burning process. The compacted and stable char can effectively stop the heat and mass transfer resulted in protecting the materials under the char.

The I_D/I_G ratio follows the order of TPEE/P-N/CNTs/MoS$_2$ (1.76)<TPEE/P-N/CNTs (1.81) <TPEE/P-N (2.38), Formulation 4 has the highest I_D/I_G ratio value indicating it has the most thermally stable char structure. The result corresponds with the morphology of char residue. There is not much big difference in the I_D/I_G ratio value between Formulation 3 and Formulation 4 for that the Mo element catalyze the char forming process resulted in the production of more amorphous carbon on the surface than the graphited carbon in the inner part. Adding the CNTs can enhance the graphitization of the char for the network structure has the benefit for the inner pressure which is important to the graphitization process. The combiniation of CNTs and MoS$_2$ can build a new network structure which can

improve the degree of the graphitization. Meanwhile, the Mo element catalyzed the char forming process. The graphited carbon filled into the pore of the network structure and large amount of amorphous carbon dispersed on the surface of the layer to effectively prevent the melt dripping behavior.

4. Conclusion

In this work, the melt dripping behavior was disappeared for adding the combination of CNTs and MoS2 into P-N flame retarding TPEE during the burning process. The TGA results suggested the addition of CNTs obviously decreased the weight of char residues at the high temperature. Otherwise, the introduction of 1 wt% MoS_2 effectively increased the char residue. The FTIR indicated that the metal ions on the surface of the CNTs can catalyze the decomposition process of TPEE while Mo element can catalyze the cycloaddition interaction of the double-bonding product which can promote additional carbonaceous char at the high temperature. SEM images and Raman spectra presented that a compacted char was formed through the introduction the combination of CNTs and MoS_2 into P-N flame retarding TPEE. During the burning process, the Mo element catalyzes the cycloaddition process of volatile decomposition products which formed amorphous carbon to cover on the surface of CNTs. TPEE/P-N/CNTs/MoS_2 can effectively build the network to decrease the decomposition rate and the addition of MoS_2 can eliminate the harmful effect resulted from the introduction of CNTs. CNTs and MoS_2 had a synergistic effect on the char forming process and anti-dripping behavior.

Reference

1   Alosime EM, Edwards GA, Martin DJ. Structure-property relationships in copolyester elastomer-layered silicate nanocomposites. *Journal of Applied Polymer Science* **2015**;132(13).

2   Lilaonitkul A, Cooper S. Properties of polyether-polyester thermoplastic elastomers. *Rubber Chemistry and Technology* **1977**;50(1):1-23.

3   Qunzhao ZXMNZ, Tao J. Preparation and Properties of PBT/PTMG Block Poly (ether ester) with Different Molar Ratio of BDO. *Chinese Journal of Materials Research* **2013**;2:008.

4   Szymczyk A, Senderek E, Nastalczyk J, Roslaniec Z. New multiblock poly (ether-ester) s based on poly (trimethylene terephthalate) as rigid segments. *European Polymer Journal* **2008**;44(2):436-43.

5   Guan J, Sacks MS, Beckman EJ, Wagner WR. Biodegradable poly (ether ester urethane) urea elastomers based on poly (ether ester) triblock copolymers and putrescine: synthesis, characterization and cytocompatibility. *Biomaterials* **2004**;25(1):85-96.

6   Su Y, Yu J, Wang Y, Zhu J, Hu Z. Effect of hard segment length on the properties of poly (ether ester) elastomer prepared by one pot copolymerization of poly (ethylene glycol) and cyclic butylene terephthalate. *Journal of Polymer Research* **2015**;22(10):1-10.

7   Papke N, Karger-Kocsis J. Thermoplastic elastomers based on compatibilized poly (ethylene terephthalate) blends: effect of rubber type and dynamic curing. *Polymer* **2001**;42(3):1109-20.

8   Broza G, Schulte K. Melt processing and filler/matrix interphase in carbon nanotube reinforced poly (ether-ester) thermoplastic elastomer. *Polymer Engineering & Science* **2008**;48(10):2033-38.

9   Huang X, Lin S, Shang J, He W, Lan J. Mechanical, thermal, and ultraviolet resistance properties of poly (ether–ester)/cerium oxide (CeO2) composite fibers. *Journal of Reinforced Plastics and Composites* **2014**;33(13):1207-15.

10   Zhong Y, Wu W, Wu R, Luo Q, Wang Z. The flame retarding mechanism of the novolac as char agent with the fire retardant containing

phosphorous–nitrogen in thermoplastic poly (ether ester) elastomer system. *Polymer Degradation and Stability* **2014**;105:166-77.

11 You G, Cheng Z, Tang Y, He H. Functional Group Effect on Char Formation, Flame Retardancy and Mechanical Properties of Phosphonate–Triazine-based Compound as Flame Retardant in Epoxy Resin. *Industrial & Engineering Chemistry Research* **2015**;54(30):7309-19.

12 Wang B, Tai Q, Nie S, Zhou K, Tang Q, Hu Y, et al. Electron beam irradiation cross linking of halogen-free flame-retardant ethylene vinyl acetate (EVA) copolymer by silica gel microencapsulated ammonium polyphosphate and char-forming agent. *Industrial & Engineering Chemistry Research* **2011**;50(9):5596-605.

13 Gong J, Niu R, Wen X, Yang H, Liu J, Chen X, et al. Synergistic effect of carbon fibers and carbon nanotubes on improving thermal stability and flame retardancy of polypropylene: a combination of a physical network and chemical crosslinking. *RSC Advances* **2015**;5(8):5484-93.

14 Sonnier R, Bokobza L, Concha-Lozano N. Influence of multiwall carbon nanotube (MWCNT) dispersion on ignition of poly (dimethylsiloxane)–MWCNT composites. *Polymers for Advanced Technologies* **2015**;26(3):277-86.

15 Shi Y, Long Z, Yu B, Zhou K, Gui Z, Yuen RK, et al. Tunable thermal, flame retardant and toxic effluent suppression properties of polystyrene based on alternating graphitic carbon nitride and multi-walled carbon nanotubes. *Journal of Materials Chemistry A* **2015**;3(33):17064-73.

16 Robertson J. Realistic applications of CNTs. *Materials Today* **2004**;7(10):46-52.

17 Bianco A, Kostarelos K, Prato M. Applications of carbon nanotubes in drug delivery. *Current opinion in chemical biology* **2005**;9(6):674-79.

18 Liu Z, Chen K, Davis C, Sherlock S, Cao Q, Chen X, et al. Drug delivery with carbon nanotubes for in vivo cancer treatment. *Cancer research* **2008**;68(16):6652-60.

19 Sun Z, Yuan H, Liu Z, Han B, Zhang X. A Highly Efficient Chemical Sensor Material for H~ 2S: alpha-Fe~ 2O~ 3 Nanotubes Fabricated Using Carbon Nanotube Templates. *ADVANCED MATERIALS-DEERFIELD BEACH THEN WEINHEIM-* **2005**;17(24):2993.

20 Jang Y-T, Moon S-I, Ahn J-H, Lee Y-H, Ju B-K. A simple approach in fabricating chemical sensor using laterally grown multi-walled carbon nanotubes. *Sensors and Actuators B: Chemical* **2004**;99(1):118-22.

21 Zhang M, Su L, Mao L. Surfactant functionalization of carbon nanotubes (CNTs) for layer-by-layer assembling of CNT multi-layer films and fabrication of gold nanoparticle/CNT nanohybrid. *Carbon* **2006**;44(2):276-83.

22 Qi P, Vermesh O, Grecu M, Javey A, Wang Q, Dai H, et al. Toward large arrays of multiplex functionalized carbon nanotube sensors for highly sensitive and selective molecular detection. *Nano letters* **2003**;3(3):347-51.

23 Mittal G, Dhand V, Rhee KY, Park S-J, Lee WR. A review on carbon

nanotubes and graphene as fillers in reinforced polymer nanocomposites. *Journal of Industrial and Engineering Chemistry* **2015**;21:11-25.

24   Drakonakis VM, Aureli M, Doumanidis CC, Seferis JC. Modulus–density negative correlation for CNT-reinforced polymer nanocomposites: Modeling and experiments. *Composites Part B: Engineering* **2015**;70:175-83.

25   Beyer G. Short communication: carbon nanotubes as flame retardants for polymers. *Fire and materials* **2002**;26(6):291-93.

26   Ma HY, Tong LF, Xu ZB, Fang ZP. Functionalizing carbon nanotubes by grafting on intumescent flame retardant: nanocomposite synthesis, morphology, rheology, and flammability. *Advanced functional materials* **2008**;18(3):414-21.

27   Zhang Q, Zhan J, Zhou K, Lu H, Zeng W, Stec AA, et al. The influence of carbon nanotubes on the combustion toxicity of PP/intumescent flame retardant composites. *Polymer Degradation and Stability* **2015**;115:38-44.

28   Shen Y, Gong W, Xu Y, Zheng B. Preparation of multi-walled carbon nanotubes and its application as flame retardant for polypropylene. *Micro & Nano Letters, IET* **2015**;10(11):625-29.

29   Peeterbroeck S, Laoutid F, Swoboda B, Lopez-Cuesta JM, Moreau N, Nagy JB, et al. How carbon nanotube crushing can improve flame retardant behaviour in polymer nanocomposites? *Macromolecular rapid communications* **2007**;28(3):260-64.

30   Rao BN, Praveen T, Sailaja R, Khan MA. HDPE nanocomposites using nanoclay, MWCNT and intumescent flame retardant characteristics. Paper presented at: Properties and Applications of Dielectric Materials (ICPADM), 2015 IEEE 11th International Conference on the, 2015.

31   Isitman NA, Kaynak C. Nanoclay and carbon nanotubes as potential synergists of an organophosphorus flame-retardant in poly (methyl methacrylate). *Polymer Degradation and Stability* **2010**;95(9):1523-32.

32   Ye L, Wu Q, Qu B. Synergistic effects and mechanism of multiwalled carbon nanotubes with magnesium hydroxide in halogen-free flame retardant EVA/MH/MWNT nanocomposites. *Polymer Degradation and Stability* **2009**;94(5):751-56.

33   Beyer G. Filler blend of carbon nanotubes and organoclays with improved char as a new flame retardant system for polymers and cable applications. *Fire and materials* **2005**;29(2):61-69.

34   Liu H, Si M, Deng Y, Neal AT, Du Y, Najmaei S, et al. Switching mechanism in single-layer molybdenum disulfide transistors: an insight into current flow across Schottky barriers. *ACS nano* **2013**;8(1):1031-38.

35   Konarova M, Tang F, Chen J, Wang G, Rudolph V, Beltramini J. Nano-and Microscale Engineering of the Molybdenum Disulfide-Based Catalysts for Syngas to Ethanol Conversion. *ChemCatChem* **2014**;6(8):2394-402.

36   Wan S, Li Y, Peng J, Hu H, Cheng Q, Jiang L. Synergistic Toughening of Graphene Oxide–Molybdenum Disulfide–Thermoplastic Polyurethane Ternary Artificial Nacre. *ACS nano* **2015**;9(1):708-14.

37　Sorrentino A, Altavilla C, Merola M, Senatore A, Ciambelli P, Iannace S. Nanosheets of MoS2-oleylamine as hybrid filler for self-lubricating polymer composites: Thermal, tribological, and mechanical properties. *Polymer Composites* **2015**.

38　Zhang H, Lu S, Zheng J, Du J, Wen S, Tang D, et al. Molybdenum disulfide (MoS 2) as a broadband saturable absorber for ultra-fast photonics. *Optics express* **2014**;22(6):7249-60.

39　Yan R, Simpson JR, Bertolazzi S, Brivio J, Watson M, Wu X, et al. Thermal conductivity of monolayer molybdenum disulfide obtained from temperature-dependent Raman spectroscopy. *ACS nano* **2014**;8(1):986-93.

40　Zhou F, Xin S, Liang HW, Song LT, Yu SH. Carbon nanofibers decorated with molybdenum disulfide nanosheets: synergistic lithium storage and enhanced electrochemical performance. *Angewandte Chemie International Edition* **2014**;53(43):11552-56.

41　Wang D, Song L, Zhou K, Yu X, Hu Y, Wang J. Anomalous nano-barrier effects of ultrathin molybdenum disulfide nanosheets for improving the flame retardance of polymer nanocomposites. *Journal of Materials Chemistry A* **2015**;3(27):14307-17.

42　Zhou K, Zhang Q, Liu J, Wang B, Jiang S, Shi Y, et al. Synergetic effect of ferrocene and MoS 2 in polystyrene composites with enhanced thermal stability, flame retardant and smoke suppression properties. *RSC Advances* **2014**;4(26):13205-14.

43　Jiang S-D, Tang G, Bai Z-M, Wang Y-Y, Hu Y, Song L. Surface functionalization of MoS 2 with POSS for enhancing thermal, flame-retardant and mechanical properties in PVA composites. *RSC Advances* **2014**;4(7):3253-62.

44　Zhou K, Yang W, Tang G, Wang B, Jiang S, Hu Y, et al. Comparative study on the thermal stability, flame retardancy and smoke suppression properties of polystyrene composites containing molybdenum disulfide and graphene. *RSC Advances* **2013**;3(47):25030-40.

45　Zhong Y, Li M, Zhang L, Zhang X, Zhu S, Wu W. Adding the combination of CNTs and MoS 2 into halogen-free flame retarding TPEE with enhanced the anti-dripping behavior and char forming properties. *Thermochimica Acta* **2015**;613:87-93.

Figure Captions

Fig.1 FTIR spectra of the solid pahse in TPEE(a), TPEE/P-N(b), TPEE/P-N/CNTs(c), TPEE/P-N/CNTs/MoS$_2$(d) at different temperatures.

Fig.2 Mechanism of the Mo element catalyazation of char forming process

Fig.3 Gas chromatogram of the gaseous pyrolysis products of TPEE(a), TPEE/P-N(b), TPEE/P-N/CNTs(c), TPEE/P-N/CNTs/MoS$_2$(d) obtained on heating at 600 $^{\circ}$C.

Fig.4 Mass loss(a) and mass loss rate(b) curves of samples recorded under air atmosphere, heating rate 10 $^{\circ}$C min^{-1}.

Fig.5 SEM images of the residue for TPEE/P-N(a), TPEE/P-N/CNTs(b), TPEE/P-N/CNTs/MoS$_2$(c)

Fig.6 Raman curves of the char residues of TPEE/P-N, TPEE/P-N/CNTs, TPEE/P-N/CNTs/MoS$_2$ after calcinations at 800 $^{\circ}$C for 10 min.

(a)
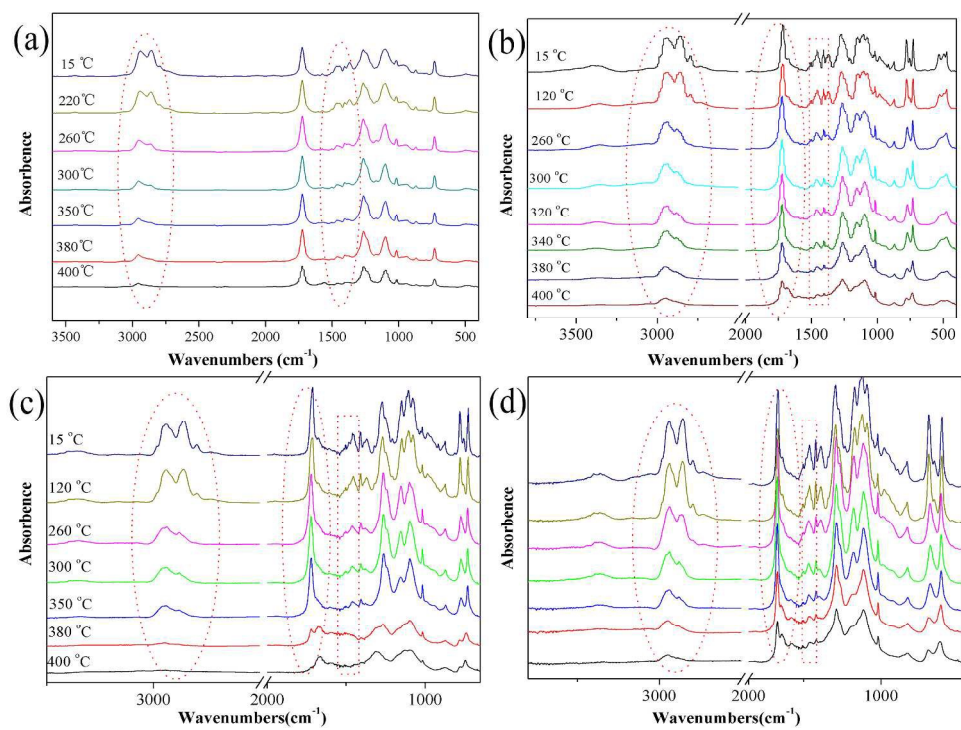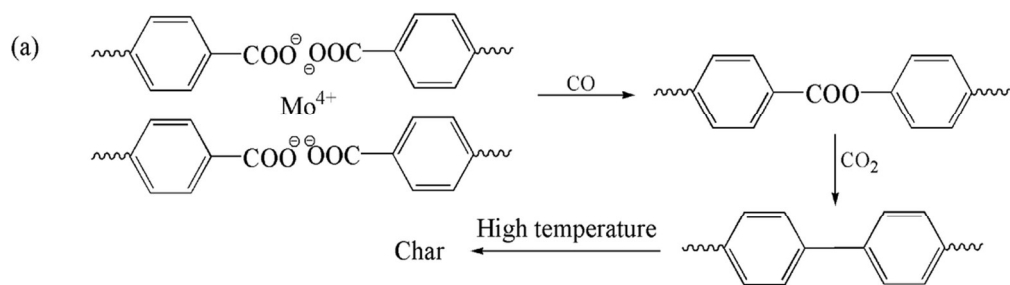
Lewis base-acid interaction

(b)
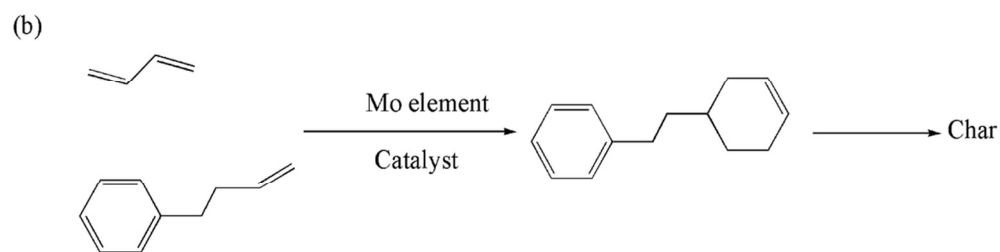
Cycloaddition interaction

49x35mm (600 x 600 DPI)
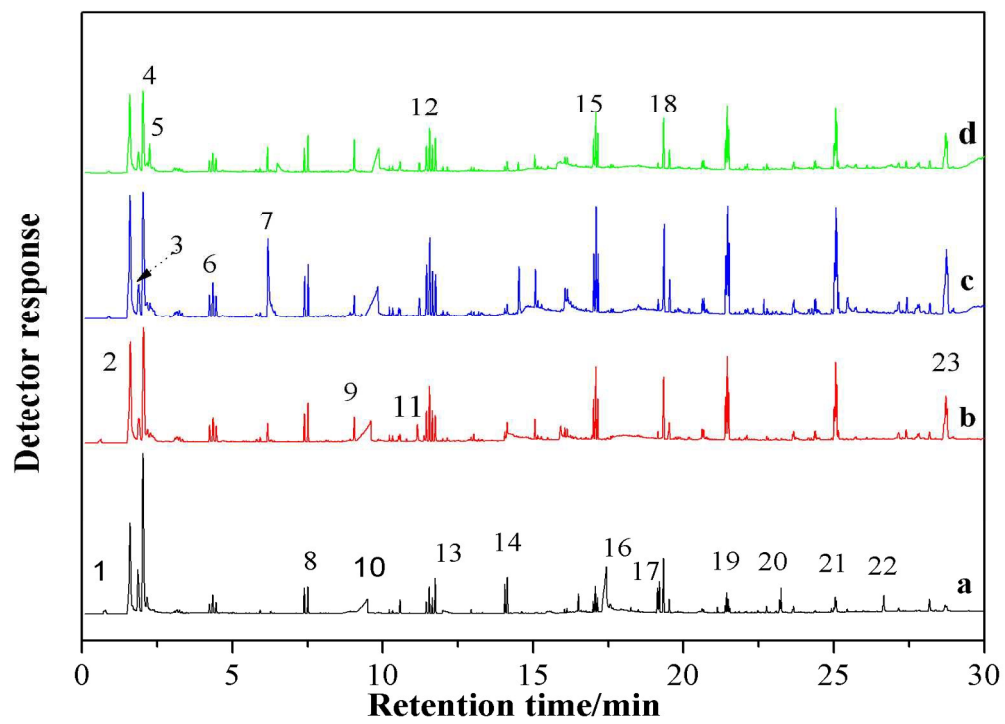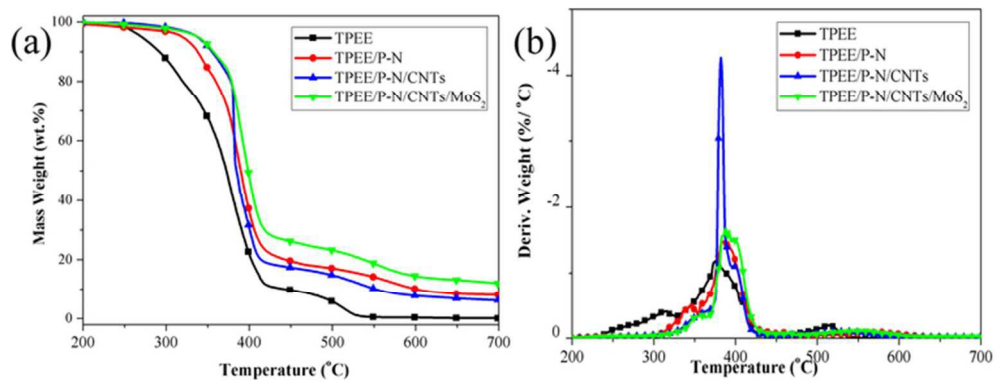
64x25mm (300 x 300 DPI)
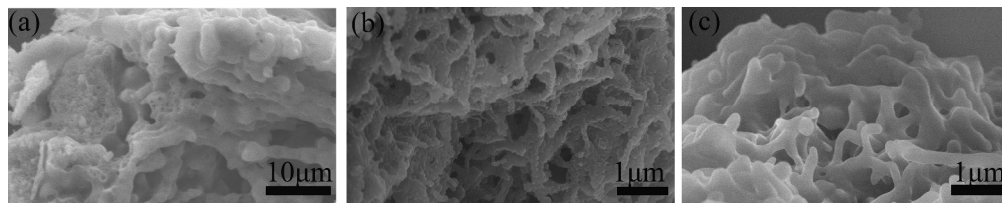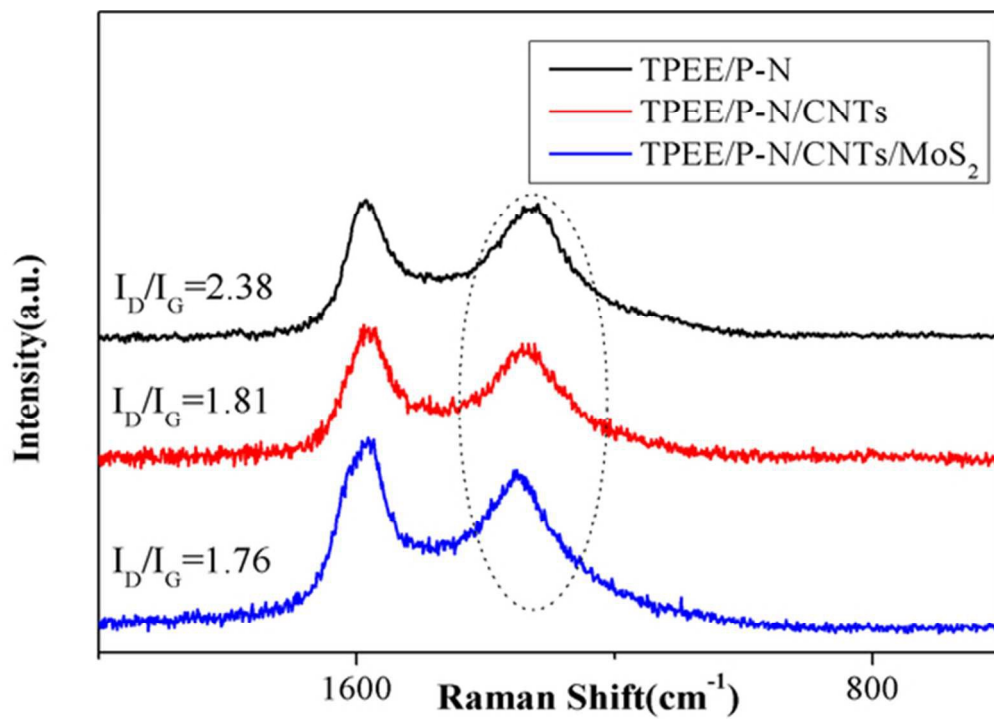
49x35mm (300 x 300 DPI)

Table 1. Composition of formulation in wt%

	Material	TPEE	P-N	CNTs	MoS$_2$
1	TPEE	100	_	_	_
2	TPEE/P-N	85	15	_	_
3	TPEE/P-N/CNTs	82	15	3	_
4	TPEE/P-N/ CNTs/MoS$_2$	81	15	3	1

Table 2. Results of UL-94 tests of the investigated formulations

	Material	Ranking	Dripping
1	TPEE	No rating	_ [a]
2	TPEE/P-N	V-2	No/yes[b]
3	TPEE/P-N/CNTs	V-2	Yes/yes
4	TPEE/P-N/CNTs/MoS	V-0	No/no

[a] the specimen burns out with dripping behavior

[b] No/yes corresponds to the first/second flame application.

Table 3. The arrtribution of wavenumbers of characteristic peaks obtained for the all

forumations [7,19]

Wavenumbers of Characteristic peaks (cm^{-1})	Attribution
3413 cm^{-1}	-OH, MPP
2956cm^{-1}, 2861cm^{-1}	-CH$_2$, stretching vibration
1715 cm^{-1}	-C=O, stretching vibration
1458cm^{-1}	-CH$_2$, scission vibration
1411 cm^{-1}	aromatic ring
1270 cm^{-1}	-CO-O esters
1100 cm^{-1}	-CH$_2$-O-CH$_2$- ether
1150 cm^{-1},1079 cm^{-1},780 cm^{-1}	-P-O
1013 cm^{-1}	-PO$_4^{3-}$
727 cm^{-1}	-CH bending vibration of aromatic ring
531 cm^{-1}	O-P-O, MPP
474 cm^{-1}	O=P-O, AlPi

Table 4.The pyrolysis products of Formulation 1-4 at 600 ℃.

No	Molecular mass (m/z)	Retention time (min)	Compound
1	44	0.785	CO_2
2	54	1.602	1,3-butadiene
3	70	1.865	2,3-dihydrofuran
4	72	2.037	tetrahydro-furan
5	72	2.171	3-buten-1-ol
6	127	4.351	4-butoxy-1-butene
7	103	6.16	benzonitrile
8	100	7.514	2,3-dimethyl pentane
9	147	9.1	4-cyanobenzoic acid
10	128	9.49	benzoic acid
11	59	11.1	guanidine
12	202	11.6	1,4-butanediol diglycidyl ether
13	164	11.7	benzenebutanoic acid
14	186	14.1	heptan-2-yl butanoate
15	170	17.1	3-butoxy-2,4-dimethyl-1-pentene
16	250	17.4	2-hexan-3-yloxycarbonylbenzoic acid
17	100	19.2	cis-3-methylpent-3-ene-5-ol
18	278	19.4	dibutyl terephthalate
19	286	21.4	2,2,4-trimethyl-1,3-pentanediol diisobutyrate

20	100	23.7	z-1-methoxy-2-pentene
21	396	25.1	bis(2-ethylhexyl) ester
22	206	26.7	3-hydroxy-2-methyl-1-phenyl-hexan-1-one
23	334	28.8	2-ethylhexyl-2-methylpropyl phthalate

Table.5 Characteristic mass peaks (M_n<100) and relative peak area of Formulation 1-4.

Products	Rentention time	1(%)	2(%)	3(%)	4(%)
1,3-butadiene	1.602	13.72	11.01	8.14	6.06
2,3-dihydrofuran	1.865	5.762	2.429	2.152	1.927
Tetrahydro-furan	2.037	17.48	9.315	6.3	6.285
benzoic acid	9.49	5.42	5.44	4.9	5.207